INVESTIGATION OF THE FERMI SURFACE OF TIN BY THE SIZE EFFECT

V. F. GANTMAKHER

Institute for Physics Problems, Academy of Sciences, U.S.S.R.

Submitted to JETP editor September 26, 1962

J. Exptl. Theoret. Phys. (U.S.S.R.) 44, 811—822 (March, 1963)

The size effect observed in measurements of the dependence of surface resistance on magnetic field strength at helium temperatures for frequencies 1—5 Mc was used to study the Fermi surface of tin. Detailed data on the sizes of extremal electron orbits in momentum space were obtained for magnetic field directions lying in the (100) and (110) planes. The results are compared with the nearly free-electron model.

THE size effect observed when the surface resistance $Z = R + iX$ of a metal in a magnetic field is measured at relatively low radio frequencies provides a convenient new method for studying Fermi surfaces.[1] The magnetic field is applied parallel to the surface of a sample in the form of a plane parallel plate; the planes containing the electron orbits in momentum space are perpendicular to the surface. It appears from qualitative considerations that when the mean free electron path l is sufficiently long, then for the field H_0, in which electron trajectories lying in the extremal cross section of the Fermi surface fit exactly within the plate, touching both surfaces, the magnetic-field dependence of impedance should exhibit a singularity. The singularity is associated with the fact that in large fields electrons return to the skin layer more than once, contributing to the conductivity each time, while in weak fields they are scattered at the crystal surface during their first orbital revolution.

The electronic equation of motion $\dot{\mathbf{p}} = -(e/c)\,\mathbf{v} \times \mathbf{H}$ shows that the electron orbit in momentum space and the projection of the electron trajectory in configuration space on a plane perpendicular to $\mathbf{H}$ are similar and are rotated relative to each other through the angle $\pi/2$ (Fig. 1). By integrating this equation over time, it is easy to relate the field H_0 and the plate thickness d to the width 2p of the electron orbit in momentum space in a direction perpendicular to the magnetic field and to the normal on the plane of the plate:[2]

$$2p = \frac{e}{c} Hd \qquad (1)$$

(the coefficient 2 is introduced for convenience, since in most cases extremal electron orbits in momentum space have a center of symmetry). A and B are the tangential points.

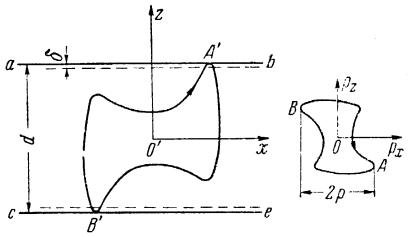

FIG. 1. Electron trajectory in configuration space (left) for the size effect, and the corresponding orbit in momentum space. The magnetic field is perpendicular to the plane of the drawing: ab and ce are the boundaries of the sample.

EXPERIMENT

If surface scattering is to make an appreciable contribution to the surface resistance, an electron must be able to complete several revolutions in its trajectory within its mean free path. This condition is represented by the inequality $l \gg d$. On the other hand, it is easily seen that because of the finite skin depth δ the singularity cannot be very sharp and must be spread through the width $\Delta H/H_0 \sim \delta/d$, because the centers of orbits contributing to the effect are determined only with accuracy within δ. Therefore the condition $\delta/d \ll 1$ must be satisfied. These two relations determine the range of possible sample thicknesses.

A technique developed earlier for preparing cast samples in removable quartz forms[3] using tin containing 10^{-4}% impurities tentatively,[4] makes mean free paths of the order 10^{-1} cm possible. However, for tin at frequencies $f \sim 10^6$ cps we have $\delta \sim 10^{-4}$ cm. Accordingly, we selected the thickness range 0.2—0.6 mm for our samples. (With thinner samples greatly increased difficulties are encountered in connection with preparing precise samples, measuring their thickness, handling them during mounting etc.) The samples were

disks 18 mm in diameter; the crystallographic orientations of normals to the surface was determined within 1°.

The ratio δ/d can be reduced by increasing the generator frequency, although this is not effective in the case of the anomalous skin effect, because $\delta \sim f^{-1/3}$. The upper frequency limit is determined by the quasi-static requirement that during the time t of an electron revolution in its orbit the electric field should not change appreciably:

$$t \ll 1/f. \tag{2}$$

Then each time the electron returns to the skin layer it encounters a high-frequency electric field in practically the same phase as during its previous traversal of the skin layer.

At higher frequencies, when (2) is no longer satisfied, it is also possible to observe effects determined by the relations between the trajectory size and the sample size, [2,5] although in this case they are complicated by phase relations. Moreover, the sharply nonmonotonic shape of the Z(H) curves due to cyclotron resonances hinders the observance of size effects.

We selected the frequency range 1—5 Mc, which satisfies (2) and is very convenient for experimental purposes. The sample was placed within a measuring coil (1 in Fig. 2) forming part of the rf generator circuit and consisting of about 50 turns of copper wire 50μ in diameter wound to form a single layer. The sensitivity of the method was enhanced by reducing as much as possible the gap between the sample surface and the turns of the coil. For this purpose the coil was made rectangular but frameless, having rigidity provided only through the use of BF-2 adhesive. The space factor K (the ratio of the magnetic flux passing through the metal to the entire flux through the coil) was easily determined from the relative frequency change as a sample becomes superconducting:

$$K \approx 2\Delta f/f \approx 0.004. \tag{3}$$

Sample 2 lay freely on two pieces of paper glued to the quartz plate 3 flush with the coil winding. The foamed polystyrene plates 4 limited the motion of 3 along the coil axis, while strips of cigarette paper 5 glued to the edges of the sample prevented it from turning. The plate 3 rested on foamed polystyrene lugs 6 cemented to the endface of the quartz tube 7, which was fastened to a copper disk 8 by means of two bronze springs. The entire device was placed inside a copper can which contained a heat-exchanger gas and was immersed in liquid helium.

The coil was connected to the generator, which was located on the lid of the helium Dewar, by means of a stainless steel rod lying along the tube axis and sealed by polystyrene-foam disks. Throughout most of the experimental work the amplitude of the high-frequency magnetic field was maintained at 0.2—0.4 Oe.

The block diagram Fig. 3 shows that the experimental work consisted in two-coordinate registration of $\partial f/\partial H$ as a function of H. In our work the former quantity was directly proportional to the derivative of the imaginary part of the impedance with respect to the field:

$$\partial f/\partial H = -\alpha \partial X/\partial H \tag{4}$$

($\alpha > 0$ and depends on space factor K of the coil).[1)]

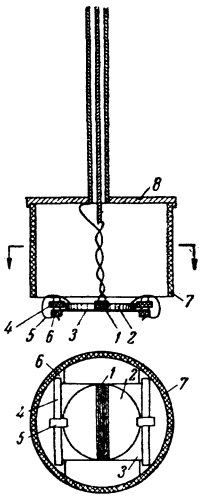

FIG. 2. Low-temperature portion of the measuring generator.

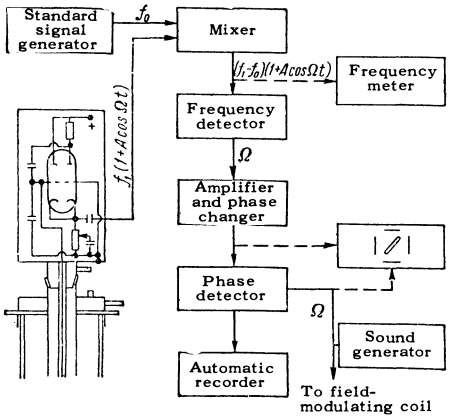

FIG. 3. Block diagram of apparatus.

[1)]The effect could also be studied by measuring $\partial R/\partial H$ using the standard apparatus for nuclear magnetic resonance. We note that since the position of the line in the size effect is independent of frequency the functions R(H) and X(H) are not interrelated through differential expressions arising out of the Kramers-Kronig relations as in the case of resonance effects.[6]

The modulation frequency of the constant magnetic field was 20 cps. In the high-purity samples required for our work the skin depth for the modulating field at this frequency is estimated to be about 0.2—0.5 mm, which is comparable with the sample thickness. The modulation amplitude in most experiments did not exceed 0.5 Oe.

RESULTS

We investigated the extremal cross sections of the Fermi surface subject to the condition that the magnetic field lies in one of the two planes (010) and ($\bar{1}10$). (The normals **n** to the surfaces of the samples coincided with the corresponding crystallographic directions [010] or [$\bar{1}10$].) In these planes 26 different groups of extremal cross sections were observed.

The size-effect lines in Figs. 4 and 5 exhibit changes of position, intensity, and shape as the field direction is varied. In view of the absence of any theoretical calculations, we determined H_0 for each line from the most characteristic position of the line, usually from its sharpest extremum. This uncertainty, which is associated essentially with the diversity of line shapes, has a varying

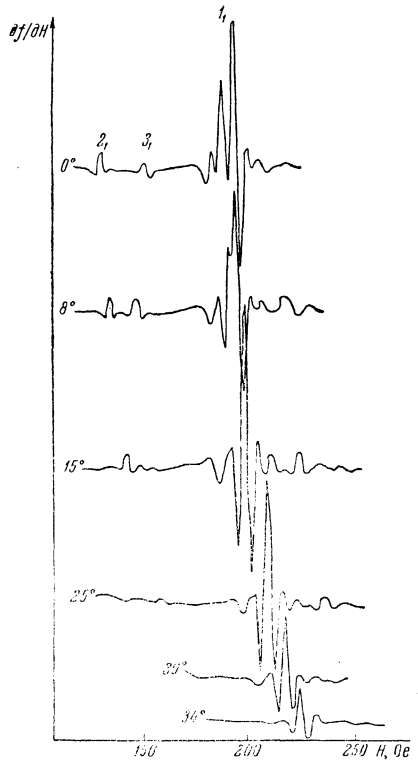

FIG. 4. Size-effect lines for a sample with **n** ∥ [010], d = 0.39 mm, rf field **E** ∥ [100], T = 3.8°K, f = 3.0 Mc. The left-hand end of each curve is marked with the angle between the field **H** and the [001] axis. The numerals 1_1, 2_1, 3_1 are the numbers of the cross sections corresponding to Fig. 7.

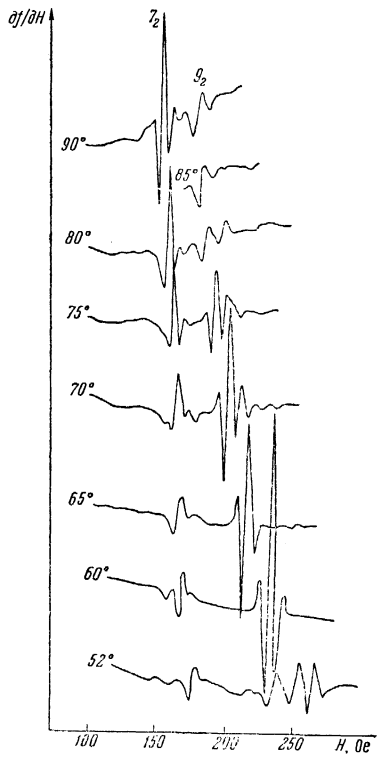

FIG. 5. Size-effect lines for a sample with **n** ∥ [$\bar{1}$10], d = 0.40 mm, **E** ∥ [001], T = 3.8°K, f = 3.1 Mc. The numerals 7_2 and 9_2 are the numbers of the cross sections corresponding to Fig. 8.

effect that sometimes amounts to 5%. Otherwise the absolute accuracy of the measurements would be determined from the accuracy of sample thickness measurements and would be about 2—3%.

Figure 6 shows the wide diversity of line shapes, regarding which the following rules can be stated. The shape of a line (1) is repeated from sample to sample independently of their thickness; (2) is independent of the polarization of the electric field when the latter is rotated within at least the limits ± 50° from the most favorable observation position; (3) is insensitive to changes of the surface state (following the etching of one sample neither the shape nor the intensity of the lines was affected).

All results obtained in the study of the extremal cross sections are collected in Figs. 7 and 8, which show the dependence of p/p_0 on direction; p was taken from (1), and $p_0 = 2\pi\hbar/a = 11.4 \times 10^{-20}$ g-cm/sec is the boundary momentum of the Brillouin zone in the [100] direction. All calculations and constructions were based on the following data: at 4° K, a = 5.80 Å, a/c = 1.84, and the radius of the free-electron sphere in momentum space is 1.52 p_0. The parameters of the tin lattice at helium temperatures were determined from the Grüneisen

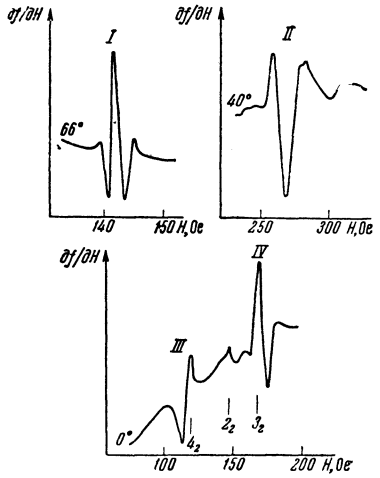

FIG. 6. Different types of size-effect lines. I – n ∥ [010], d = 0.39 mm, E ∥ [100], cross section 4_1; II – n ∥ [$\bar{1}$10], d = 0.40 mm, E ∥ [110], cross section 1_2; III, IV – n ∥ [$\bar{1}$10], d = 0.40 mm, E ∥ [001]. All curves were plotted for T = 0.8°K, f = 3.1 Mc.

rule.[4] In Figs. 7 and 8 the centers of all extremal orbits coincide with the coordinate origin, independently of their actual (unknown) positions within the Brillouin zone. The curves obtained in this manner will be called cross sections, although, as will be shown subsequently, they are not always cross sections of the Fermi surface. The subscript 1 following the number of a cross section in the following discussion will denote Fig. 7; the subscript 2 will denote Fig. 8.

The numbers enclosed by parentheses in Fig. 7 refer to curves characterizing the effective-mass anisotropy of the corresponding regions of the Fermi surface; these were taken from Fig. 4 of [7] on cyclotron resonance. An almost complete one-to-one correspondence between our results and those of Khaĭkin was established by comparing the angular intervals within which cyclotron resonance and the size-effect lines were observed. The good correspondence of these intervals suggests that both cyclotron resonance and the size effect were observed practically as long as the corresponding orbits existed at all. In cross sections 1_1 and 7_1 Khaĭkin observed the cutting-off of cyclotron resonance,[2] permitting the simultaneous measurements of momentum and the effective mass.

The different symbols used in Figs. 7 and 8 denote different types of lines. In some cases, however, the line shape was intermediate between the given types. Some lines were very complex, with two or three approximately equal peaks; this has been noted by two (or three) points for the cross sections 4_1, 11_1, and 9_2. The possible causes will be discussed below. The superposition of lines sometimes prevented interpretation of the results; this is indicated by dashed lines in the diagrams. These uncertainties will probably be eliminated by investigating samples having a longer mean free path.

Figures 7 and 8 do not indicate the line intensities. However, for a single sample at a given temperature the intensities vary from cross sec-

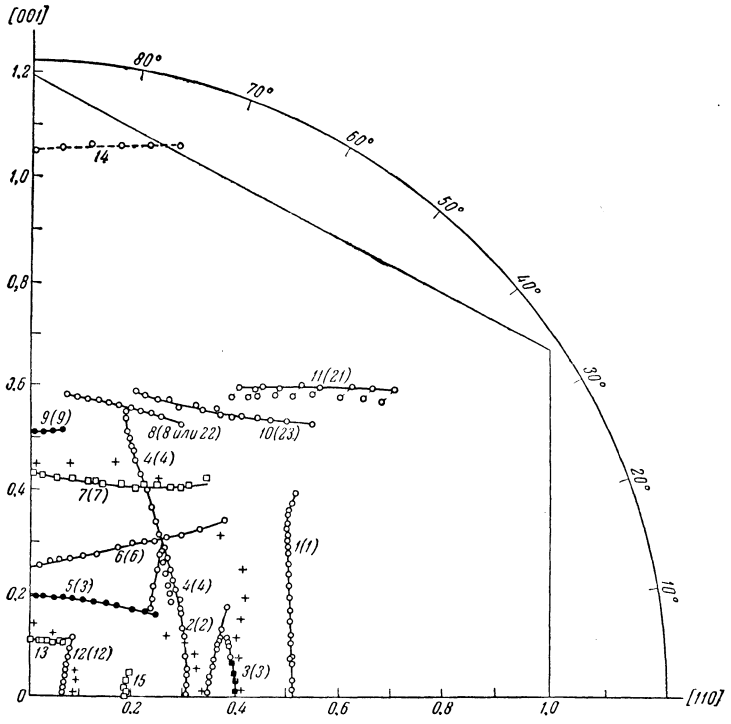

FIG. 7. Anisotropy of the half-widths of extremal orbits in the (010) plane. The different symbols denote different types of lines corresponding to Fig. 6: ○ – type I, ● – II, □ – III, ■ – IV; + denotes data in[11]. The light continuous line is the central cross section of the Brillouin zone.

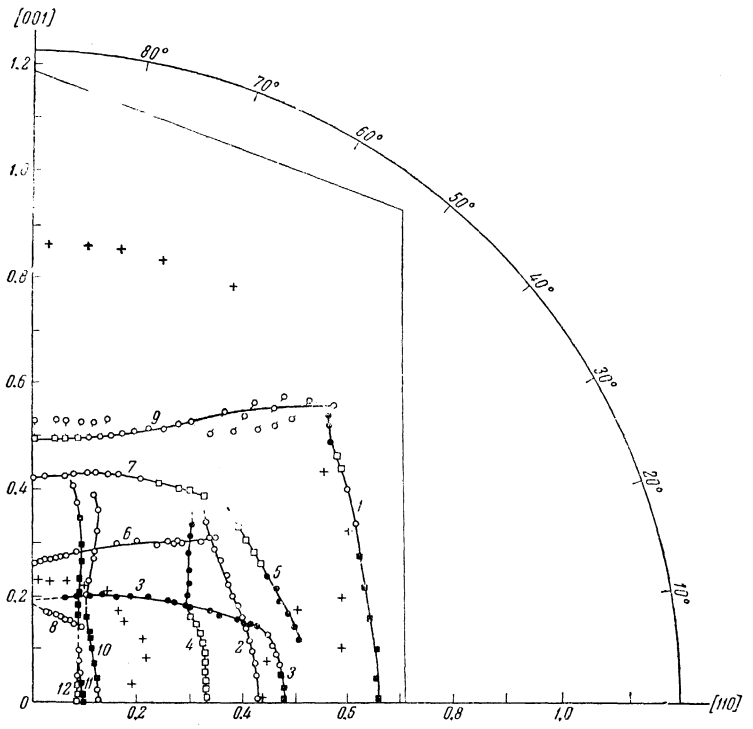

FIG. 8. Anisotropy of the half-widths of extremal orbits in the ($\bar{1}10$) plane. The notation is the same as in Fig. 7.

tion to cross section within a range of two orders of magnitude. The most intense lines pertain to cross sections 1_1, 1_2, 7_2, and 9_2. Somewhat less intense lines pertain to cross sections 4_1 (in the range 70—50°), 10_1, and 11_1. Line 14_1 is much less intense and more diffuse, and was therefore plotted arbitrarily.

The line intensity depends on the polarization of the electric field; observation of the effect requires a component of the electron velocity along the electric field while traversing the skin layer. Therefore, for example, the cross sections 1_1—4_1, 12_1, and 15_1 are not seen for $\mathbf{E} \parallel [001]$, while the other cross sections are not seen for $\mathbf{E} \parallel [100]$. The same applies to the ($\bar{1}10$) plane.

In order to avoid overcrowding the figures and thus complicating the examination of our results, we did not number the samples nor indicate how many samples were associated with the various cross sections. The size effect was observed in 9 samples altogether. In all cases the results for samples of a single given orientation agreed, although the intensities and diffuseness of the lines varied, depending on sample thickness and probably on insufficiently controlled defects originating in the course of preparation. One sample of each orientation was investigated in detail.

As was noted in [8], the size effect can also be observed in multiple fields (multiples of H_0); we observed this only for cross sections 1_1 and 7_2. It is interesting that the effect in multiple fields can probably be associated with more than the line intensity. In Fig. 5 lines 7_2 and 9_2 are approximately of the same intensity. However, for the 7_2 lines the effect is observed in multiple fields within the angular range 90—70°, while for the 9_2 lines the effect is not observed at any angle.

DISCUSSION OF RESULTS

In attempting to use our results for the purpose of determining the shape of the Fermi surface it must be remembered that the extremal orbits exhibiting the size effect can have extremely diversified shapes (Fig. 9). A curve in Fig. 7 or Fig. 8 represents the Fermi-surface cross section directly only when the surface region of interest gives type a orbits for which the point O coincides with the center of the Brillouin zone. If the point O is located elsewhere in the Brillouin zone the

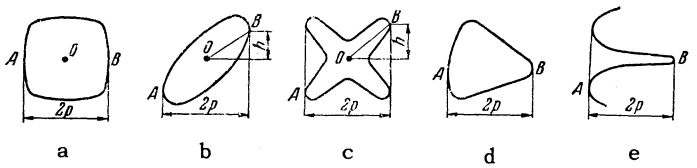

FIG. 9. Possible arrangements of the tangential points of electron orbits. The magnetic field is perpendicular to the plane of the figure.

experimental line must be suitably translated. For example, 15_1 can be shifted along the [001] axis to coincide with the uppermost points of 4_1. On the other hand, it is seen from the shape of 4_1, that for **H** ∥ [001] this part of the Fermi surface has only maximal, but no minimal, orbits. This portion of the surface contains tangential points of extremal orbits for two entirely different magnetic-field directions, as is shown in two places on our diagram. If the corresponding region of the Fermi surface is nearly cylindrical, the minimal and maximal orbits are similar and the two lines merge into a single complex line. This accounts for the existence of two maxima for 1_1 lines in fields close to the [001] direction (Fig. 4) and also, probably, for the complex shape of 4_1 lines (in the interval 32—40°), 9_2 (around 50°; Fig. 5), and 11_1.

For extremal orbits of types b and c the situation is complicated by the fact that the straight line connecting the orbital center and the tangential point is not perpendicular to the tangent, and the distance h can vary with the field direction. Then the corresponding tangential points on the Fermi surface lie on a nonplanar line. Cases d and e (the latter for open orbits) are even more complicated when the orbits have no center of symmetry.

The Fermi surface of tin has been studied by many investigators.[5,7,9-11] Most authors compare their results with the nearly free-electron model. However, it must be noted that data on the de Haas—van Alphen effect,[9] and galvanomagnetic[10] and ultrasonic[11] measurements, do not definitely determine the extent to which this model represents tin. This occurs because of the complexity of the surface, the low accuracy of measurements, and the fact that the very character of the measured quantities (the areas of extremal cross sections, the directions of orbital trajectories) often hinders detailed comparisons. The first serious proof that this model gives for tin a picture that is close to reality is found essentially only in[5]; yet even here this proof pertains to only part of the surface of one zone (zone 4(a) in Fig. 10).

The character of our results—the linear dimension of the extremal orbit—and the attained accuracy and sensitivity permit a more detailed comparison with the model than for any of the previously known methods. Figure 10 shows constructions based on the nearly free-electron model by Harrison's method.[12] These differ from the Gold and Priestly constructions[9] only in so far as, wherever possible, we refrained from rounding off sharp corners at the surface. Some additional information regarding the nearly free-electron model

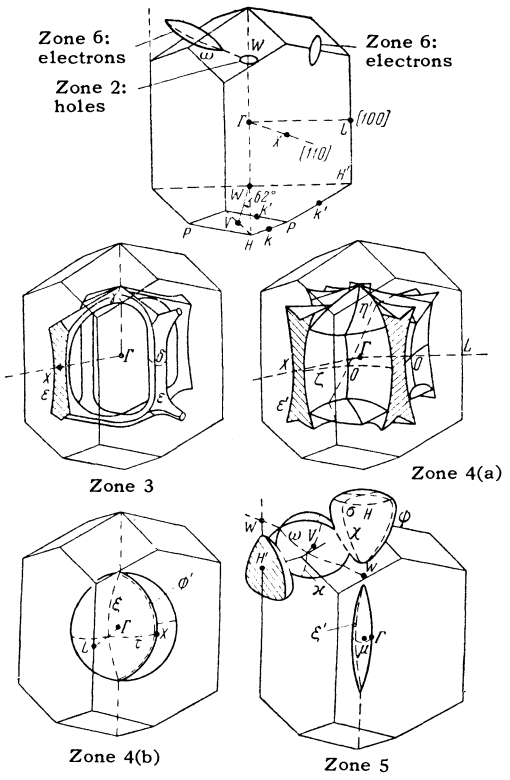

FIG. 10. Fermi surface of tin according to the nearly free-electron model.

(compared with[9]) will be mentioned subsequently.

We shall begin with zone 4(a), whose cross section can be identified relatively reliably. This includes, first of all, cross sections 1_1 and 1_2 (the orbits ξ in Fig. 10), 9_1 and 9_2 (the orbits ϵ'), and 8_1 and 11_1 (the orbits η'). These experimental points are compared in Fig. 11 with two cross sections of the nearly free-electron model, the centers of the orbits coinciding with the corresponding center of surface symmetry. Very good agreement is observed when 1_1 and 2_1 are compared with the construction. The remaining points should fit on the outer contour of the construction. We also note that the presence of projections on the connecting regions between separate sheets of the surface must lead to the result that for some magnetic-field directions there will be additional extremal orbits whose planes will not contain the center of symmetry. Therefore as a confirmation of the model we can regard, in addition to the approximately equal momenta, the complex line shapes of 9_2 and 11_1 (the existence of some extrema for certain fields) and the appearance of 10_1.

We can thus regard the existence of the 4(a) surface as experimentally confirmed. To be sure, this does not apply to the curvature of separate regions of the surface. For example, the radius of curvature of a surface around the point O in the cross

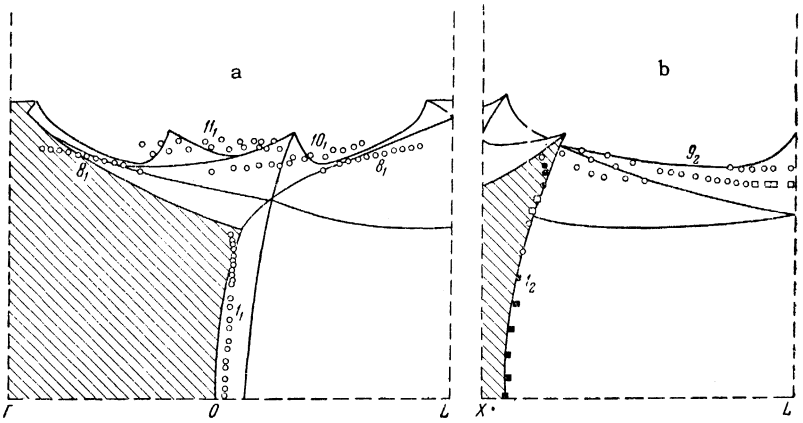

FIG. 11. Comparison of experimental results with the nearly free-electron model for zone 4a. a – cross section by the plane ΓHVH'L. The orbital center of 1_1 is the point L. The orbital centers of 8_1, 10_1, and 11_1 – the point Γ of the neighboring Brillouin zones – are also projected on L. Of these cross sections centered on the point Γ of the given zone only 8_1 is represented in the figure. b – cross section by the plane XLH'P. The orbital center of 1_2 is the point L; that of 9_2 is the point X projected on L. The shaded areas are not occupied by electrons.

section by the (100) plane is approximately 2.5 times greater than in the construction, although the point O is located far from the bent lines on the constructed surface. (At the same time, the cross section 1_2, which coincides with a bent line, agrees very well with the construction.)

The cross sections 3_1, 5_1, and 3_2 define a rather large closed surface. The break between 3_1 and 5_1 should probably be attributed to the low signal intensity; according to Khaĭkin [7] the corresponding effective-mass curve is bent but not broken off at 16°. The dimensions of this surface in the (001) plane are in very good agreement with the construction for zone 4(b), but its height (i.e., the dimension along [001]) is only one-third as large. Therefore there is some uncertainty about identifying this surface with the 4(b) surface of the model (although this identification is most probably correct). One of the other possibilities is the the (3_1, 5_1, 3_2) surface is associated with some other zone of the nearly free-electron model such as the sixth zone, but that the 4(b) zone must be identified with a surface giving the cross sections 7_1, 7_2, and 5_2.

Figure 10 shows that the orbits δ of zone 3 do not each separately exhibit fourth-order symmetry. The symmetry results from their relative positions in the reciprocal lattice. In the field **H** ∥ [001] for a sample with **n** ∥ [010] all these orbits yield an identical distance between the tangential points (cross section 12_1), while for a sample with **n** ∥ [110] the orbits are divided into two groups, each associated with a different distance between the tangential points (11_2 and 12_2; Fig. 12). The area of the cross section constructed through the points of 11_2 and 12_2 is $0.0155\,(2\pi\hbar/a)^2$; Gold and Priestly obtained $0.014\,(2\pi\hbar/a)^2$. [9]

The plot shows that the inclined tubes in the third zone are narrow, having a width of approximately $0.03 \times 2\pi\hbar/a$ at the narrowest point. The very small deformation of the Fermi surface can cause

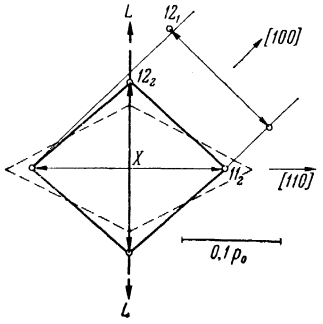

FIG. 12. The orbit 3δ. The dashed line is the nearly free-electron model. LXL is the Brillouin zone boundary.

these connecting regions to break off and greatly change the surface topology. Therefore the angular dependences of 11_2 and 12_2, which suggest closed surfaces, do not seriously conflict with the model. It should be noted that because of insufficiently long mean free paths or insufficiently accurate sample orientation the resolution of the 8_2, 10_2, 11_2, and 12_2 lines in the range 45—65° was very poor. Therefore the angular dependences of these cross sections are not entirely clear. For example, the 10 line may possibly end somewhere around ~50° or go over into 8_2, while 11_2 and 12_2 diverge above 55°. Nevertheless, we believe that there are grounds for stating that the third zone consists of separate surfaces extended along the [001] axis (two surfaces for each Brillouin zone) but not interconnected.

We turn finally to zone 5 of the nearly free-electron model, which, according to the construction, consists of small surfaces at the centers of the zones extended in the [001] direction and very complex open multiply-connected surfaces located in the upper and lower parts of the zones. An open surface consists of large pear-shaped surfaces arranged in a checkerboard pattern (with narrow ends pointing upward and downward alternately) and connected by inclined surfaces centered on the points V, like the surfaces of zone 4(b), which can be

Direction of magnetic field	S*	Direction of measured orbital half-width	p/p_0 according to construction	Available experimental values of p/p_0	Remarks
[001]	~0.4	[100]	0.47	0.35 (2_1)	5 σ (Fig. 10)
		[110]	0.58	0.43 (2_2)	
[100]	0	[001]	0.41		5 ψ »
	0	[001]	0.24	0.42 (7_1)	5 ω »
	~0.1	[001]	~0.25	0.25 (6_1)	Open orbits
	0.5	[001]	0.4		5 κ (Fig. 10)
[110]	0	[001]	0.41	0.42 (7_2)	5 χ »

*S is the distance from the center of the zone to the plane containing the extremal cross section.

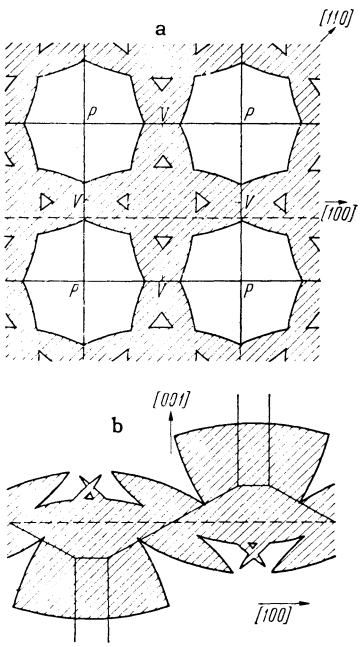

FIG. 13. Nearly free-electron model. Two cross sections of the open part of zone 5: a – a cross section by the (001) plane passing through the points P and V; b – cross section by the (100) plane, 0.1 p_0 from the center of the zone. The dashed line in cross section a represents the intersecting plane of cross section b, and vice versa. The thin continuous lines represent the intersections of the plane with the Brillouin zone boundaries. The shaded region is occupied by electrons.

pictured as a cruciform intersection of two convex lenses. Two lobes of the cruciform surfaces correspond to each of the four sides of every "pear." Figure 13 shows two cross sections of this surface; the table gives the dimensions of its principal extremal cross sections in the case when the magnetic field is along the principal crystal axes. The fact that this surface includes a layer of open trajectories in the [100] direction (Fig. 13b) is an additional proof of its existence in tin; according to [10] this layer should exist, while according to Khaĭkin's [5] and our measurements it is not in zone 4(a). The width of the shaded cross section in the [100] direction in Fig. 11a is everywhere smaller than $p_0/2$.

The fifth column of the accompanying table gives the experimental data, which agree well with the calculations. However, we believe that it is premature to discuss the degree to which our results coincide with the model constructions in zone 5. The structure of the zone is very complex and small deformations of individual regions can result in significant topological changes. Therefore for the purpose of arriving at an exact and unique conclusion very much more than the presently available information is needed here; this also applies, to some degree, to the other results. We hope, however, than an investigation of the extremal cross sections as the field is rotated in other crystallographic planes, especially in the (001) plane, will make it possible to construct a complete Fermi surface for tin.

In discussing the results of the present work we have used only data concerning anisotropy as given in Figs. 7 and 8. It can be expected that theoretical calculations of the size effect will enable us to relate intensity and line shape to the dispersion law close to the tangential points of extremal cross sections, thus greatly facilitating the construction of the Fermi surface from the size effect.

The author is deeply grateful to Yu. V. Sharvin for daily guidance, to M. S. Khaĭkin and R. T. Mina for valuable discussions, and to A. I. Shal'nikov for his interest.

[1] V. F. Gantmakher, JETP **42**, 1416 (1962), Soviet phys. JETP 15, 982 (1962).

[2] M. S. Khaĭkin, JETP **41**, 1773 (1961), Soviet Phys. JETP **14**, 1260 (1962).

[3] Yu. V. Sharvin and V. F. Gantmakher, PTÉ (in print).

[4] V. B. Zernov and Yu. V. Sharvin, JETP **36**, 1038 (1959), Soviet Phys. JETP **9**, 737 (1959).

[5] M. S. Khaĭkin, JETP **43**, 59 (1962), Soviet Phys. JETP **16**, 42 (1963).

[6] G. E. Pake and E. M. Purcell, Phys. Rev. **74**, 1184 (1948).

[7] M. S. Khaĭkin, JETP **42**, 27 (1962), Soviet Phys. JETP **15**, 18 (1962).

[8] V. F. Gantmakher, JETP **43**, 345 (1962), Soviet Phys. JETP **16**, 247 (1963).

[9] A. V. Gold and M. G. Priestley, Phil. Mag. **5**, 1089 (1960).

[10] N. E. Alekseevskiĭ and Yu. P. Gaĭdukov, JETP **41**, 1079 (1961), Soviet Phys. JETP **14**, 770 (1962).

[11] T. Olsen, in The Fermi Surface, W. A. Harrison and M. B. Webb (eds.), John Wiley and Sons, New York, 1960, p. 237.

[12] W. A. Harrison, Phys. Rev. **116**, 555 (1959).

Translated by I. Emin
137